

ENERGY-BASED ERROR CONTROL STRATEGIES SUITABLE  
FOR LONG MD SIMULATIONS

by

Kante Easley

A thesis submitted in conformity with the requirements  
for the degree of Master of Science  
Graduate Department of Computer Science  
University of Toronto

Copyright © 2009 by Kante Easley

# **Abstract**

Energy-Based Error Control Strategies Suitable  
for Long MD Simulations

Kante Easley

Master of Science

Graduate Department of Computer Science

University of Toronto

2009

When evaluating integration schemes used in molecular dynamics (MD) simulations, energy conservation is often cited as the primary criterion by which the integrators should be compared. As a result variable stepsize Runge-Kutta methods are often ruled out of consideration due to their characteristic energy drift.

We have shown that by appropriately modifying the stepsize selection strategy in a variable stepsize RK method it is possible for the MD practitioner to obtain substantial control over the energy drift during the course of a simulation. This ability has been previously unreported in the literature, and we present numerical examples to illustrate that it can be achieved without sacrificing computational efficiency under currently obtainable timescales.

## **Acknowledgements**

Foremost, I would like to thank my supervisor Wayne Enright for his patience and excellent guidance. I'd like to thank Christina Christara for her useful feedback. Finally, I would like to thank my parents for their continuous support.

# Contents

<b>1</b>	<b>Introduction</b>	<b>2</b>
1.1	Motivation . . . . .	2
1.2	Background . . . . .	3
1.2.1	Molecular Dynamics . . . . .	3
1.2.2	Runge-Kutta Methods . . . . .	6
1.3	Previous Work . . . . .	11
1.4	Contribution of the Thesis . . . . .	11
1.5	Outline of the Thesis . . . . .	12
<b>2</b>	<b>The Simple System</b>	<b>13</b>
2.1	Description . . . . .	13
2.1.1	The Potential Function . . . . .	13
2.1.2	Computational Tricks . . . . .	14
2.1.3	Reduced Units . . . . .	15
2.1.4	Initial Conditions and Equilibration . . . . .	16
2.2	Numerical Results . . . . .	17
2.2.1	Traditional Methods . . . . .	18
2.2.2	Behavior of the Energy Drift . . . . .	20
<b>3</b>	<b>An Improved Energy Drift Control</b>	<b>22</b>
3.1	The Algorithms . . . . .	23

3.1.1	Simple Energy Error Control . . . . .	23
3.1.2	Adjusting the error estimate . . . . .	26
3.1.3	A further adjustment . . . . .	28
3.1.4	Higher order methods . . . . .	31
<b>4</b>	<b>PBC and cutoffs</b>	<b>34</b>
4.1	Description . . . . .	34
4.2	Potential Cutoff Scheme . . . . .	36
4.2.1	Standard Integrators . . . . .	37
4.2.2	Novel Integrators . . . . .	39
4.3	Force cutoff . . . . .	40
4.3.1	Standard Integrators . . . . .	41
4.3.2	Novel Integrators . . . . .	42
4.4	$C^\infty$ cutoffs . . . . .	43
<b>5</b>	<b>Conclusions and Future Work</b>	<b>46</b>
5.1	Summary . . . . .	46
5.2	Future Work . . . . .	47

# List of Tables

2.1	Conversions between commonly used quantities in reduced, and the International System of Units (SI). . . . .	16
2.2	Stepsize and RMS Energy Error for Standard RK Methods . . . . .	19
3.1	Scaled stepsize, RMS error, and maximum energy drift for the benchmark Verlet method and the simple stepsize selection strategy applied with rkd56. . . . .	24
3.2	Scaled stepsize, RMS error, and maximum energy drift for the benchmark Verlet method and the adjusted stepsize selection strategy (3.3) used with rkd56. . . . .	27
3.3	Scaled stepsize, RMS error, and maximum energy drift for the benchmark Verlet method and the stepsize selection strategy (3.4) applied for rkd56. . . . .	31
3.4	Scaled stepsize, RMS error, and maximum energy drift for the benchmark Verlet method and the stepsize selection strategy (3.3) applied with rkd78. . . . .	33
4.1	Results for the Verlet and rkd56 methods with a potential cutoff function. Both the true, and modified energy are presented for comparison. . . . .	39
4.2	Performance of novel integration schemes using a potential cutoff . . . . .	40
4.3	Results for the Verlet and rkd56 methods with a force cutoff function. Both the true and modified energy are presented for comparison. . . . .	42
4.4	Performance of novel integration schemes using a force cutoff . . . . .	42
4.5	Performance of novel integration schemes using a $C^\infty$ potential cutoff . . . . .	45

# List of Figures

2.1	Typical energy conservation using Stormer-Verlet integration. . . . .	19
2.2	Characteristic energy drift typically associated with standard Runge-Kutta methods. . . . .	20
2.3	Energy drift for various values of $TOL$ . . . . .	21
3.1	Energy drift observed with the novel stepsize selection in rdk56. . . . .	25
3.2	Energy drift using the stepsize selection strategy (3.3). . . . .	28
3.3	Energy drift using the stepsize selection strategy (3.4) with $N_{\text{int}} = 100$ . . . . .	30
3.4	Energy drift using the 8th order RK method rkd78 and the stepsize selection strategy (3.3). . . . .	32
4.1	Periodic boundary conditions. As the shaded atom leaves the simulation box it's mirror image from the adjacent cell enters, maintaining a constant number of particles at all times. . . . .	35
4.2	Plot of the potential cutoff function with $r_{on} = 1$ and $r_{off} = 2$ . . . . .	36
4.3	Modified energy drift (top) and true energy drift (bottom) using the Verlet integrator (left) and the rkd56 integrator (right) using the potential cutoff scheme with $r_{on} = 12\text{\AA}$ and $r_{off} = 16\text{\AA}$ . . . . .	38
4.4	The smooth $C^\infty$ cutoff function (top) and the standard potential cutoff function (bottom). . . . .	44

# Chapter 1

## Introduction

### 1.1 Motivation

Molecular dynamics (MD) simulation is a commonly used tool for investigating the detailed behavior of macromolecular systems. Computing the forces involved in these large systems comprises 90% of the computational work in a typical simulation, and must be done several times on each timestep in the integration of the system of underlying ordinary differential equations. This computational cost is compounded by the huge number of steps that must be taken to accurately determine a solution over a meaningful timescale. Thus, increasing the effective size of the timestep is an obvious way to reduce the computational burden of MD simulations.

One of the primary criterion in choosing an integrator for molecular dynamics simulation is energy conservation [10], [5], [17]. Because of their simplicity and energy conservation properties, lower order symplectic methods are most commonly used by current practitioners of MD, with the second-order Verlet method being most often used in practice [14]. Since standard Runge Kutta methods tend to exhibit systematic energy drift when integrating MD systems they have largely been excluded from consideration as a viable method in the literature.

This thesis demonstrates that although standard Runge Kutta integrators do not intrinsically

conserve energy, by taking advantage of variable stepsize with novel stepsize selection mechanisms they are able to faithfully and efficiently compute long term MD simulations. Further, they do this with energy drifts comparable to standard symplectic methods at currently attainable timescales. However, the relationship between tolerance and energy conservation is far from clear, making standard RK methods potentially unfavorable to the MD practitioner. In order to address this difficulty new stepsize selection strategies are proposed that provide the simulator with the ability to predictably control the energy drift while maintaining competitive computational costs.

## 1.2 Background

### 1.2.1 Molecular Dynamics

At the most fundamental level a molecular dynamics simulation solves the initial value problem

$$\dot{y} = f(t, y), y(0) = y_0, t \in (0, t_{\text{end}}), \quad (1.1)$$

where the trajectories of  $N$  particles are determined by Newton's equations of motion.

We use  $q(t) = (q_1(t), \dots, q_N(t))$  and  $v(t) = (v_1(t), \dots, v_N(t))$  to represent the positions and velocities of the system of  $N$  particles, respectively. It is important to note that each  $q_i, v_i$  consists of a triplet of values  $q_i = (q_{ix}, q_{iy}, q_{iz}), v_i = (v_{ix}, v_{iy}, v_{iz})$  containing the  $x, y$  and  $z$  coordinates of each particle so that the "path"  $y(t) = (q(t), v(t))$  obtained by solving equation 1.1 lies in  $\mathbb{R}^{6N}$ . Such a path is subsequently referred to as the *phase space trajectory* of a system consisting of  $N$  particles in the *phase space*  $\mathbb{R}^{6N}$ .

With this notation, any linear operator  $A : \mathbb{R}^N \rightarrow \mathbb{R}^N$  acting on  $q$  or  $v$  should be understood as  $Aq \stackrel{\text{def}}{=} A \otimes I_3 q$ , or  $Av \stackrel{\text{def}}{=} A \otimes I_3 v$  where  $\otimes$  is the Kronecker product and  $I_3$  is the  $3 \times 3$  identity matrix. It will usually be clear from context how to treat a general operator acting on  $q$  or  $v$ , and any case where a potential ambiguity arises will be explained in detail. With care, the notational savings afforded by these conventions more than outweigh the few difficulties that

may arise.

Using this notation Newton's equations of motion for the system described by equation 1.1 take on the specific form,

$$\begin{aligned}\dot{q} &= v, \\ \dot{v} &= M^{-1}F(q),\end{aligned}\tag{1.2}$$

with

$$M^{-1} = \begin{bmatrix} m_1^{-1} & 0 & \dots & 0 \\ \vdots & \ddots & \ddots & \vdots \\ 0 & \dots & 0 & m_N^{-1} \end{bmatrix}.$$

This system of first-order differential equations is equivalent to the more familiar,

$$F = Ma = M\ddot{q}.$$

Here,  $m_i$  is the mass of the  $i$ -th particle for  $i \in 1, \dots, N$ ,  $F$  is a force function satisfying  $F(q) = -\nabla V(q)$  for an appropriate potential function  $V$  and  $\nabla V(q)$  is the gradient  $(\frac{\partial V(q)}{\partial q_1}, \dots, \frac{\delta V(q)}{\delta q_N})^T$ . With the choice of a reasonable potential function integrating Newton's equations of motion can provide a realistic approximation to the real phase space trajectory of the system.

A typical example of the intermolecular potential function used in current MD simulations consists of the sum of a short range Van der Waals potential, and a long range Coulombic interaction <sup>1</sup>

$$V(r) = \sum_{i=1}^N \sum_{j>i} \phi(r_{ij}) + \sum_{i=1}^N \sum_{j>i} \frac{Q_i Q_j}{\epsilon r_{ij}}\tag{1.3}$$

where  $r_{ij} \stackrel{\text{def}}{=} \|q_i - q_j\|$  for the  $l_2$  norm  $\|x\| \stackrel{\text{def}}{=} \sqrt{x \cdot x}$  and  $Q_i$  gives the electric charge of the  $i$ th particle. The choice of  $Q_i$ ,  $Q_j$  and the parameters defining  $\phi(r)$  are chosen to match the physical characteristics of the material being modeled subject to computational efficiency

---

<sup>1</sup>If intramolecular forces are considered this expression becomes more complicated. The nature of the force function is not the focus of this thesis, and the form presented herein is sufficiently general for our purposes.

considerations, and the availability of relevant empirical information. These parameters will be dealt with in more detail in subsequent sections.

Numerical results presented in subsequent sections were determined using a widely used benchmark system whose potential function contains only the Van Der Waals term, providing a realistic approximation of the intermolecular forces between argon molecules. This simple system is used when comparing integration techniques since determining a physically realistic potential for more complex systems is an active area of research, without a clearly correct choice even for slightly more complicated molecules such as water [4], [20].

### Energy Conservation

The *energy* associated with a particular phase state  $(q, v)$  is defined to be the sum of the kinetic and potential energies

$$E(q, v) = V(q) + \frac{1}{2} \sum_{i=1}^N m_i \|v_i\|^2.$$

A simple derivation shows that energy is conserved along exact solutions to equation 1.2 so long as the force function  $F$  is the exact gradient of a potential function  $V$ :

$$\begin{aligned} \frac{dE}{dt} &= \frac{dV(q(t))}{dt} + \frac{1}{2} \sum_{i=1}^N m_i \frac{d\|v_i\|^2}{dt} \\ &= \nabla V(q) \cdot \dot{q} + \frac{1}{2} \sum_{i=1}^N 2m_i v_i \dot{v}_i \\ &= \nabla V(q) \cdot v + \sum_{i=1}^N m_i v_i \frac{F_i}{m_i} \\ &= \nabla V(q) \cdot v - \nabla V(q) \cdot v = 0. \end{aligned}$$

Since the energy in an MD simulation should be constant, a common gauge of the quality of a given approximate solution is how well this quantity is preserved. The amount by which the energy changes during a simulation is known as the *energy drift*. Numerical methods generally exhibit characteristic patterns in the energy drift, with less suitable integrators having larger drifts than their more suitable counterparts. It is important to note that more accurate methods

will always exhibit reduced energy drift, but increased accuracy is not strictly necessary to obtain small drifts as can be seen from the performance of low order symplectic methods.

## 1.2.2 Runge-Kutta Methods

The non-symplectic Runge-Kutta methods we will be investigating are explicit,  $s$ -stage, order  $p$ , Runge-Kutta methods that compute an approximate solution to equation 1.1 at discrete points  $y_n \approx y(t_n)$ ,  $t_n \in [0, t_{\text{end}}]$  via the equation,

$$y_n = y_{n-1} + h_n \sum_{i=1}^s w_i k_i,$$

for  $n \in 1, 2, \dots, M$ ,  $0 = t_0 < t_1 < \dots < t_M = t_{\text{end}}$ ,  $h_n = t_n - t_{n-1}$  with,

$$k_i = f(t_{n-1} + c_i h_n, Y_i),$$

for  $i \in 1, 2, \dots, s$  and

$$Y_i = y_{n-1} + h_n \sum_{j=1}^{i-1} a_{ij} k_j.$$

The choice of the stepsize  $h_n$  and parameters  $w_j$ ,  $c_j$  and  $a_{ij}$  completely determine the approximation  $y_n$  computed at the  $n$ th timestep. If the true solution to equation 1.1 is given by  $y(t)$  then the *global error* for a  $p^{\text{th}}$  order method is defined by

$$\epsilon_n \stackrel{\text{def}}{=} \max_{n=1, \dots, N} \|y(t_n) - y_n\|,$$

and will satisfy,

$$\epsilon_n \leq \psi_n H_n^p + O(H_n^{p+1}),$$

where  $H = \max_{n=1, \dots, N} \{h_n\}$ . Given the local initial value problem,

$$\dot{z}_n = f(t, z_n(t)),$$

$$z_n(t_{n-1}) = y_{n-1},$$

we define the *local error* on step  $n$  to be,  $le \stackrel{\text{def}}{=} z_n(t_n) - y_n$ .

### Continuous Extensions and Defect Based Error Control

Standard Runge-Kutta methods only provide solution values at discrete points, while it is often desirable to provide an accurate interpolant that determines the approximate solution over the entire interval. Given solution values  $y_{n-1}, y_n$  associated with the  $n^{\text{th}}$  step, an approximation  $p_n(t)$  to the local solution for  $t \in [t_{n-1}, t_n]$  can be determined by using  $\bar{s} - s$  additional function evaluations per attempted step [7],

$$p_n(t) = y_{n-1} + h_n \sum_{j=1}^{\bar{s}} b_j(\tau) k_j. \quad (1.4)$$

Here, the  $k_1, \dots, k_s$  are determined by the RK method,  $k_{s+1}, \dots, k_{\bar{s}}$  are extra stages determined using the additional function evaluations [19] and  $b_j(\tau)$  is defined for  $t \in [t_{n-1}, t_n]$  by,

$$b_j(\tau) = \sum_{l=1}^{p+1} \beta_{jl} \tau^{l-1},$$

with

$$\tau = \frac{t - t_{n-1}}{h_n}.$$

Note that for the class of continuous extensions (the  $p_n(t)$ ) considered herein we have  $k_{s+1} = f(t_n, y_n)$  and this stage value will be the first stage of the next step so that effectively only  $\bar{s} - s - 1$  additional function evaluations are required per step to define  $p_n(t)$ .

Let  $p(t)$  denote the piecewise polynomial approximation defined by the interpolants  $p_n(t)$  associated with each step of the initial value problem 1.1. Note that  $p(t)$  is continuous and defined on the interval  $[0, t_{\text{end}}]$  since it is obtained from the all the local interpolants given by 1.4. The defect,  $\delta(t)$  of this approximate solution  $p(t)$  is then defined over the entire interval of integration as,

$$\delta(t) \stackrel{\text{def}}{=} \dot{p}(t) - f(t, p(t)).$$

It is shown in [18] that with an appropriate choice of the free parameters that define the stages  $k_{s+2}, k_{s+3}, \dots, k_{\bar{s}}$  and the  $\beta_{ij}$  the continuous approximate solution,  $p(t)$ , will satisfy,

$$\delta(t) = \Psi(\tau)h_n^p + O(h_n^{p+1}), \quad (1.5)$$

for  $t \in (t_{n-1}, t_n)$ .

Such interpolants are of optimal order and permit the use of a stepsize selection strategy designed to bound the defect over the interval  $[0, t_{\text{end}}]$ . Robust continuous Runge Kutta codes (CRKs) exist that attempt to ensure the size of the defect is bounded by a user-supplied parameter  $TOL$ . This 'backward' error control approach is advantageous in MD simulations since typical molecular models are unstable in the traditional sense and it is not feasible to specify meaningful tolerances in terms of global error for long simulations. Defect based strategies allow for the direct control of the energy drift in a simulation, as we demonstrate in subsequent sections.

### Stepsize Selection

Runge Kutta codes developed by Enright et. al. [7], [19] accept an input parameter  $TOL$  and attempt to ensure that the maximum global error over the interval of integration is less than a multiple of  $TOL$  by dynamically varying the local stepsize  $h_n = t_n - t_{n-1}$ . For continuous RK methods, the local error is estimated using an evaluation of the defect in the interval  $[t_{n-1}, t_n]$ . The quality of this estimate is dependent on where the defect is sampled and on the particular choice of interpolant polynomials. For some choices, this estimate can be asymptotically correct [12]. Estimates of the local error for more standard discrete formulas are typically determined using RK formula pairs.

If, in a given step, the local error estimate  $est_n$  satisfies  $\|est_n\| < h_n \cdot TOL$  for a discrete method, or the defect satisfies  $\|\delta(t + \tau^*h_n)\| < TOL$  for a continuous method then the step is accepted. At every accepted or rejected step,  $h_n$  is adjusted according to

$$h_{n+1} = \rho \left( \frac{TOL}{\|est_n\|} \right)^{\frac{1}{p}} h_n \quad (1.6)$$

where the constant  $\rho$  is a “safety factor” introduced to reduce the chance of a failed step<sup>2</sup>.

### Application to Molecular Dynamics

It is possible to take advantage of the estimate of the maximum magnitude of the defect to show that the energy drift in a molecular dynamics simulation can be controlled in an intuitive way. Given a specified value for  $TOL$ , a defect-based integrator provides an approximate solution  $\bar{q}(t), \bar{v}(t)$  to  $q(t), v(t)$  to problem 1.2 satisfying,

$$\begin{aligned}\dot{\bar{q}} &= \bar{v} + \delta_1, \\ \dot{\bar{v}} &= M^{-1}F(\bar{q}) + \delta_2,\end{aligned}\tag{1.7}$$

where  $\|\delta_1(t)\|$  and  $\|\delta_2(t)\|$  are both  $\leq TOL, \forall t \in [0, t_{\text{end}}]$ .

Following the derivation from section 1.2.1, one can obtain an expression for the rate of energy drift in the approximate phase space trajectory:

$$\begin{aligned}\frac{dE}{dt} &= \frac{dV(\bar{q}(t))}{dt} + \frac{1}{2} \sum_{i=1}^N m_i \frac{d\|\bar{v}_i\|^2}{dt} \\ &= \nabla V(\bar{q}) \cdot (\bar{v} + \delta_1) + \sum_{i=1}^N m_i \bar{v}_i \left( \frac{F_i}{m_i} + (\delta_2)_i \right) \\ &= \nabla V(\bar{q}) \cdot \bar{v} - \nabla V(s) \cdot \bar{v} + \nabla V(\bar{q}) \cdot \delta_1 + M\bar{v} \cdot \delta_2 \\ &= \nabla V(\bar{q}) \cdot \delta_1 + M\bar{v} \cdot \delta_2.\end{aligned}\tag{1.8}$$

Equation 1.8 provides a direct way to bound and control the energy drift during a simulation. In particular it shows that the energy drift can be controlled by appropriately controlling the magnitude of the two components of the defect in 1.7.

---

<sup>2</sup>A value of  $\rho = 0.9$  is usual

### The DVERK interface

In our investigations we use two CRK methods to illustrate our approach: `rkd56`, an implementation of an order 6 CRK method and `rkd78`, an implementation of an 8<sup>th</sup> order CRK method. Both codes were written by Enright et al. at the University of Toronto. The calling sequence for `rkd56` is:

```
subroutine rkd56 (n, fcn, x, y, xend, tol, ind, c, nw, w)
```

The calling sequence for the order 8 method is identical. When given appropriate values, the vector parameter  $c$  allows for the specification of a weighted tolerance such that the magnitude of the components of the defect of  $p_n(t)$  are controlled for  $i \in 1, 2, \dots, 6N$ . Equation 1.8 suggests that we bound the defect in equation 1.7 by,

$$\begin{aligned} \|\delta_1\| &\leq \frac{TOL}{\max_i |\nabla \bar{q}_i|}, \\ \|\delta_2\| &\leq \frac{TOL}{\max_i m_i |\bar{v}_i|}, \end{aligned}$$

so that,

$$\begin{aligned} \frac{dE}{dt} &= \nabla V(s)\delta_1 + Mw_i\delta_2, \\ \frac{dE}{dt} &\leq 3N \cdot TOL. \end{aligned} \tag{1.9}$$

On each step accepted by the integrator it is a trivial matter to implement this error control. However, evaluating the defect involves additional function evaluations which makes energy control based directly on equations 1.8 or 1.9 prohibitively expensive when applied at each time step. In chapter 2 we will demonstrate that it is possible to augment the inequality 1.6 with novel stepsize selection strategies that provide the MD practitioner with more fine-grained control over the energy drift, at a competitive computational cost.

### 1.3 Previous Work

The numerical integration of Hamiltonian systems has been an area of active research over the past 30 years. Leimkuhler's recent text [5] provides an excellent survey of the field, with a focus on molecular dynamics. There is a general consensus in the literature that symplectic integrators are superior for the long term integration of Hamiltonian systems [17]. However, for symplectic methods to preserve energy they require that a constant stepsize be used, and the computational trade-off from the restriction to a constant stepsize has not been explored in detail.

The work presented in this thesis is similar in structure to the comparisons presented in [14], [9]. In [14] Skeel and Okunbor compare the performance of symplectic and non-symplectic integrators, finding that some higher order symplectic methods allow for up to 40% increase in scaled stepsize as compared to the standard Verlet method. The possibility of exploiting optimal order continuous approximations, or variable stepsize is not considered in their investigation. The non-symplectic integrators used for comparison are run with a constant stepsize, leading to poorer performance than would be achieved from an efficient stepsize selection scheme.

Some work has also been done on the development of variable stepsize symplectic integrators [15]. These methods typically involve the modification of either the force function, or the Hamiltonian of the system in order to decompose the system into components associated with different time scales. The behavior and performance of these new methods are still being tested and they have not achieved widespread use in MD experiments.

### 1.4 Contribution of the Thesis

The primary contribution of this thesis is the development of an efficient error control schema that is able to directly bound the energy drift of a molecular dynamics simulation. It is demonstrated that even for relatively long MD simulations, our novel error control strategy is com-

petitive when compared to commonly used symplectic integrators. By modifying the stepsize selection strategies used by rkd56 and rkd78, the MD practitioner is presented with the ability to select a maximum allowable energy drift over the course of the simulation. Further, the strategies presented herein will fail early in the integration if the target drift is not achievable, allowing the practitioner to determine the appropriate integrator without wasting a substantial number of cycles.

## 1.5 Outline of the Thesis

In chapter 2 the performance of a crude error control is assessed on a problem with free boundary conditions, and a full force function. Chapter 3 outlines and tests a refinement of the error control which exploits equation (1.8) more fully. Chapter 4 tests the refined error control method against Verlet using periodic boundary conditions and a potential cutoff function; computational approximations widely used in standard MD simulations. Finally, a  $C^\infty$  cutoff function is proposed, and the error control strategies are subsequently evaluated with this cutoff. In chapter 5 the results are summarized and future work is discussed.

# Chapter 2

## The Simple System

### 2.1 Description

In order to test the efficacy of the proposed error control, a system of  $N$  non-polar atoms interacting with only the Van Der Waals force is considered. This is the simplest physically realistic system modeled using MD with generally accepted results in the literature. The test system described below is commonly used when comparing the suitability of numerical integrators for MD simulation and is the system used by Verlet [11] in introducing his famous Verlet method [14], [9].

#### 2.1.1 The Potential Function

The basic building block of the intermolecular potential for this system is the Lennard-Jones potential function (2.1), consisting of a strong repulsive term that dominates at short distances and a weak attractive term that dominates at large distances. The particular powers are chosen for computational efficiency, although the model fits empirical data closely.

$$\phi(r_{ij}) = 4\epsilon \left[ \left( \frac{\sigma}{r_{ij}} \right)^{12} - \left( \frac{\sigma}{r_{ij}} \right)^6 \right] \quad (2.1)$$

The quantities  $\epsilon$ , and  $\sigma$  represent the minimum energy of the interaction and the distance at

which the potential energy between the two particles is zero, respectively. These parameters are typically chosen to match empirical data or *ab initio* calculations and the values used here are standard for the realistic simulation of argon.

The *potential* of a system of  $N$  argon atoms in the simulation is then defined as the sum over all pairs of two particle interactions, so that (1.3) simplifies to

$$V(q) = \sum_{i=1}^N \sum_{j<i} \phi(r_{ij}).$$

In order to derive the force felt by each particle we must consider each component of the position separately. Let  $q_{3i+c}$  denote  $q_{ix}$  if  $c = 1$ ,  $q_{iy}$  if  $c = 2$  and  $q_{iz}$  if  $c = 3$ . Then the force felt by the  $c$ -th component of the  $i$ -th particle is the  $3i + c$ -th component of  $-\nabla V$ , and can be written as

$$\begin{aligned} -\nabla V_{3i+c} &= -\frac{\partial V}{\partial q_{3i+c}} \\ &= -\frac{\partial}{\partial q_{3i+c}} \sum_{j<k\leq N} \phi(r_{jk}) \\ &= -\sum_{j=i+1}^N \frac{\partial \phi(r_{ij})}{\partial q_{3i+c}} - \sum_{k=1}^{i-1} \frac{\partial \phi(r_{ki})}{\partial q_{3i+c}} \\ &= -\sum_{\substack{j=1 \\ j\neq i}}^N \frac{\partial \phi(r_{ij})}{\partial q_{3i+c}} = -\sum_{\substack{j=1 \\ j\neq i}}^N \phi'(r_{ij}) \frac{\partial r_{ij}}{\partial q_{3i+c}}, \end{aligned}$$

where  $\phi'(r_{ik}) = -48 \frac{\epsilon}{r_{ik}} \left( \left( \frac{\sigma}{r_{ik}} \right)^{12} - 0.5 \left( \frac{\sigma}{r_{ik}} \right)^6 \right)$  and  $\frac{\partial r_{ij}}{\partial q_{3i+c}} = \frac{q_{3i+c} - q_{3j+c}}{r_{ij}}$ .

Since  $\frac{q_{3i+c} - q_{3j+c}}{r_{ij}}$  is just the  $c$ -th component of the unit vector pointing from the  $i$ th atom to the  $j$ th atom, the force function  $F$ , introduced in (1.2), has the specific form:

$$F_i = \sum_{\substack{j=1 \\ j\neq i}}^N -48 \frac{\epsilon}{r_{ij}} \left( \left( \frac{\sigma}{r_{ij}} \right)^{12} - 0.5 \left( \frac{\sigma}{r_{ij}} \right)^6 \right) \frac{q_i - q_j}{\|q_i - q_j\|}.$$

## 2.1.2 Computational Tricks

There are many approximations introduced into production MD codes to increase simulation speed [17], all of which create artifacts in the conservation of energy [14]. In order to demon-

strate that the proposed techniques offer the MD practitioner with over energy drift, we will first run a simulation without the use of these time-saving devices. This will allow us to consider the effect of the numerical integration scheme as separate from the effects of extraneous modelling error.

When using the complete force calculation with no approximations it can be shown that a  $p$ th order symplectic method is able to remain within  $O(h^p)$  of the true energy, although a small systematic drift is observed over long time intervals due to roundoff error [8]. Under these conditions a non-symplectic method may have a difficult time competing with the inherent energy conservation of the symplectic Verlet method, since there will be no drift associated with force field approximations. Nevertheless, it will be shown that even over relatively long time intervals Runge-Kutta methods are able to perform comparably to the symplectic Verlet method when applied with appropriate stepsize selection strategies.

### 2.1.3 Reduced Units

In order to reduce the errors due to floating point arithmetic and for ease of coding we use reduced units in the integration. In the rescaled system,  $\sigma$ ,  $\epsilon$  and  $m$  are the fundamental units for distance, energy and mass respectively. All the atoms in our simulations have,  $m = m_{\text{argon}}$  so that in reduced units they are given unit mass.

Quantities written with the superscript \* indicate that they are expressed in reduced units. Under this system the Lennard-Jones potential (2.1) becomes,

$$\phi(r_{ij}^*) = 4 \left[ \left( \frac{1}{r_{ij}^*} \right)^{12} - \left( \frac{1}{r_{ij}^*} \right)^6 \right].$$

Table 2.1 gives the formulas used to convert between reduced and standard units [10].

	Reduced Units	SI Units
length	$r^*$	$\frac{r}{\sigma}$
energy	$e^*$	$\frac{e}{\epsilon}$
temperature	$T^*$	$\frac{k_B T}{\epsilon}$
time	$t^*$	$\frac{t}{\sigma} \sqrt{\frac{\epsilon}{m}}$
mass	$M^*$	$\frac{M}{m}$
force	$f^*$	$\frac{f\sigma}{\epsilon}$
velocity	$v^*$	$v \sqrt{\frac{m}{\epsilon}}$

Table 2.1: Conversions between commonly used quantities in reduced, and the International System of Units (SI).

### 2.1.4 Initial Conditions and Equilibration

Many of the quantities measured using the MD method require that the system satisfy the ergodic hypothesis [10]. Ergodicity is required to ensure that meaningful statements can be made about ensemble averages by computing time averages from the phase space trajectory of the system. For example, the instantaneous temperature of an MD simulation is given by,

$$T(v) = \frac{m}{3k_B N} \sum_{i=1}^N v_i^2. \quad (2.2)$$

By defining the time average for a measured quantity  $A$  as  $\langle A(t) \rangle = \frac{1}{N} \sum_{k=1}^N A(k\Delta t)$ , it is possible to define the temperature during a simulation as  $\langle T(v(t)) \rangle$ . This formula demonstrates an additional benefit of using continuous methods, as it is possible to more accurately compute time averaged quantities. That is, we are able to compute  $\langle A(t) \rangle = \frac{1}{t_{\text{end}}} \int_0^{t_{\text{end}}} A(t) dt$  to high accuracy using standard quadrature tools, rather than resorting to an unnecessarily rough partitioning of the interval  $[0, t_{\text{end}}]$ .

Since the atoms in a typical MD run are typically provided with random initial velocities and physically unlikely positions, it is necessary to allow the system to reach a more realistic

equilibrium state before useful results can be generated. In this thesis, the initial positions are set according to a face centered cubic (FCC) crystal structure, the lowest-energy static state for spherically symmetric particles. The initial width of the crystal was  $9.25^*$  as determined by a binary search to be near the width providing minimal potential energy.

Following the numerical experiments in [11], [14] the initial velocities were randomly generated with uniform distribution and scaled so that the average kinetic energy of the system was equal to the desired temperature  $T = 66\text{K}$ . The system was run for 21.66ps using the Verlet method while the temperatures were adjusted by a factor of  $\sqrt{\frac{T}{T'}}$  at each step, where  $T'$  is the measured average instantaneous temperature. After this temperature-damped equilibration the simulation progressed for an additional 2.16ps without temperature damping. The resulting phase state was used as the initial conditions for all comparative runs.

## 2.2 Numerical Results

The most expensive part of a molecular dynamics simulation is by far the evaluation of the  $O(n^2)$  force function in (1.2). These function evaluations comprise 90% of the computational effort in an MD simulation [2]. For this reason a reasonable quantity to use in comparing the efficiency of an integration scheme is the *scaled stepsize*, defined as the size of a given step divided by the number of function evaluations required to take the step [14]. Since the step sizes used in RK integrations are variable, and because some steps are rejected we use an *average scaled stepsize*,  $h_s$  to compare the computational costs of numerical integrators. Letting  $f$  be the number of function evaluations used during the integration we define  $h_s$  to be,

$$h_s = \frac{t_{\text{end}}}{f}.$$

An appropriate measure of the energy drift is given by the root-mean-square (rms) error in the energy [14], [9]:

$$\epsilon_{\text{RMS}} \stackrel{\text{def}}{=} \sqrt{\sum_t \frac{(e(t) - E)^2}{M}},$$

where  $E$  is the exact energy of the system (i.e. the energy computed at time 0) and  $e(t)$  is the energy of the system at time  $t$  as it evolves according to a particular integration scheme. The sum is taken over all  $M$  timesteps  $t_n$  ( $n = 0, \dots, M$ ) that are visited by the discrete method, so for a constant timestep scheme such as the Verlet method  $t_n \in 0, \Delta t, 2\Delta t, \dots, (M - 1)\Delta t$ .

A quantity that will be useful in subsequent sections is the following bound on the slope of the energy drift

$$\text{slope}_{\max} \stackrel{\text{def}}{=} \frac{\max_{t \in [0, t_{\text{end}}]}(e(t)) - \min_{t \in [0, t_{\text{end}}]}(e(t))}{t_{\text{end}}}.$$

It can be shown that  $\epsilon_{\text{RMS}} \leq \text{slope}_{\max}$  so that this quantity may be used as a measure of the error in the energy associated with the integration.

### 2.2.1 Traditional Methods

Figure 2.1 shows the results of a typical MD simulation using the Verlet method on a system of 864 LJ argon atoms over 2.15ns. In the majority of MD simulations the Verlet integrator is run with a constant stepsize on a femtosecond scale to provide a good trade-off between accuracy and cost [17]. All Verlet integrations in this thesis are run with a stepsize of  $1 \times 10^{-15}\text{s} = 1\text{fs}$  so that we are using the best energy conservation traditionally used in practice.

Figure 2.1 shows the characteristic behavior of the energy drift in an MD simulation when integrated using the Verlet method and the exact force calculation. The drift is highly oscillatory around a central value, with a slight systematic drift in energy over very long time intervals. The nature of the long term drift is discussed in detail in [6].

Figure 2.2 demonstrates the smooth energy drift characteristic of Runge-Kutta integrators applied to the same problem. In contrast to the Verlet method's oscillatory behavior, we see a well behaved directional drift. This systematic drift is often cited as the reason RK methods are rejected for use in long term MD simulations.

Table 2.2 reports the observed  $\epsilon_{\text{RMS}}$  and scaled stepsize for the Verlet method and this typical Runge-Kutta integrator and demonstrates that, even in the most challenging case, a variable

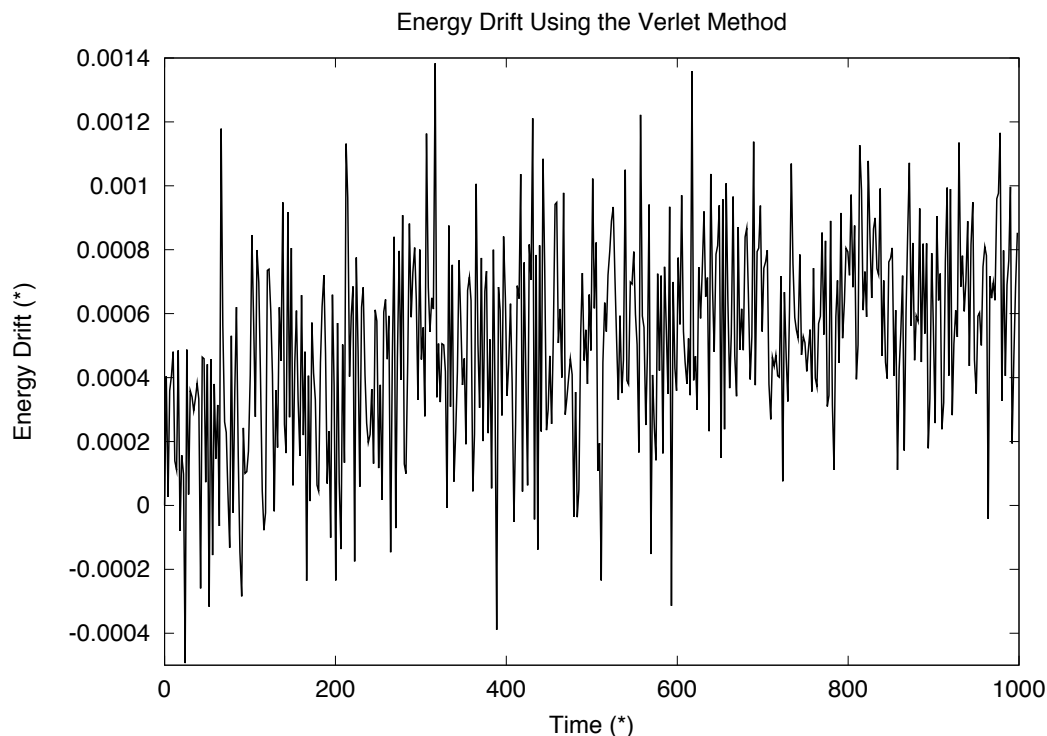


Figure 2.1: Typical energy conservation using Stormer-Verlet integration.

stepsize method can compete with Stormer-Verlet in terms of energy conservation. By supplying the Runge-Kutta code with a tolerance of  $10^{-4}$ , it was possible to obtain an average scaled stepsize comparable to the scaled stepsize used by the Verlet method. With the same computational cost it is seen that the RMS error in the energy is more than an order of magnitude smaller for the variable stepsize RK method. This performance is observed even over the relatively long time interval of 1000\* reduced units (or 2.15ns) as seen in figures 2.2 and 2.1.

	RMS Error	Scaled Stepsize
Verlet-Stormer	$5.9438 \times 10^{-4}$	$4.6294 \times 10^{-4}$
Runge-Kutta	$3.5041 \times 10^{-5}$	$3.3786 \times 10^{-4}$

Table 2.2: Stepsize and RMS Energy Error for Standard RK Methods

Comparable performance is not sufficient justification to propose using standard variable-

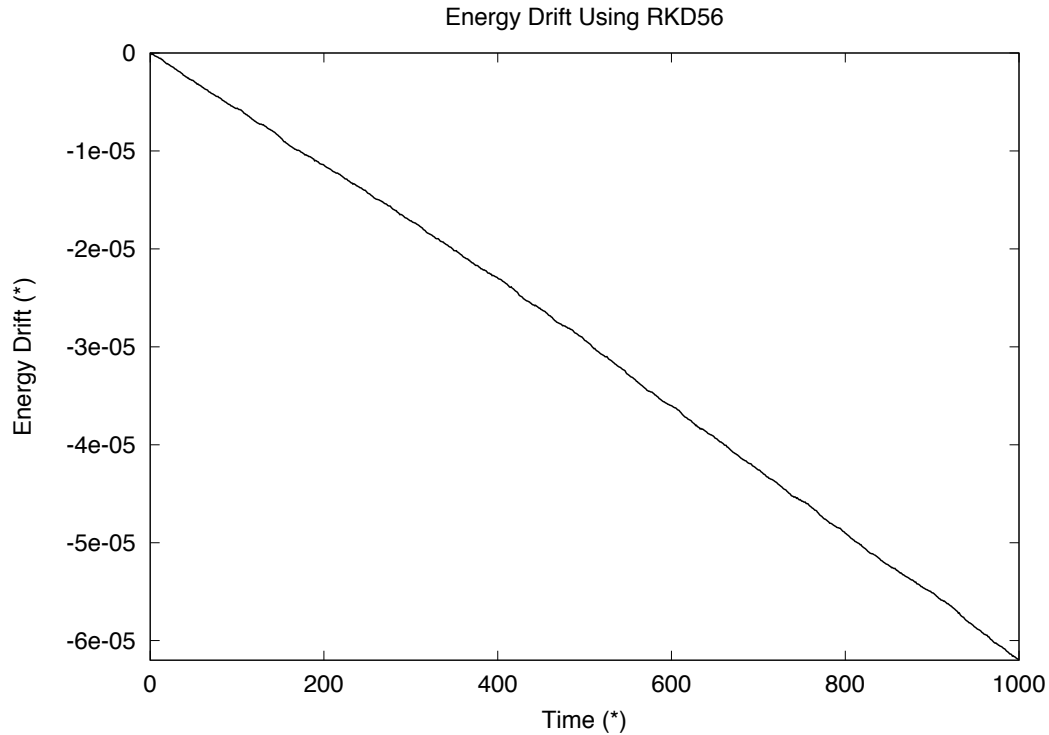


Figure 2.2: Characteristic energy drift typically associated with standard Runge-Kutta methods.

stepsize methods. First, the method of controlling the drift ( $TOL$ ) is not related to the energy drift in a simple way, so the appropriate value of  $TOL$  for a given experiment is not at all obvious. Additionally, although the RMS error can be made small for a competitive computational cost there is no guarantee that the method will be able to satisfy the error requirement with a reasonable stepsize. Moreover, a standard variable stepsize method may fail at any point during a simulation, potentially wasting a substantial amount of computer time.

### 2.2.2 Behavior of the Energy Drift

Figure 2.3 shows the drift in total energy for a variety of tolerance values over a shorter time interval. The systematic drift typical of explicit Runge Kutta methods is seen for all tolerances, and the drift varies quite predictably with respect to  $TOL$ . While there is definitely a well

behaved relationship between  $TOL$  and the energy drift, it is evident that  $TOL$  significantly overestimates the error in energy by several orders of magnitude. In the next chapter we will exploit the predictable relationship between  $TOL$  and the slope of the energy drift in order to provide the MD practitioner with increased control over over the energy drift in a typical simulation.

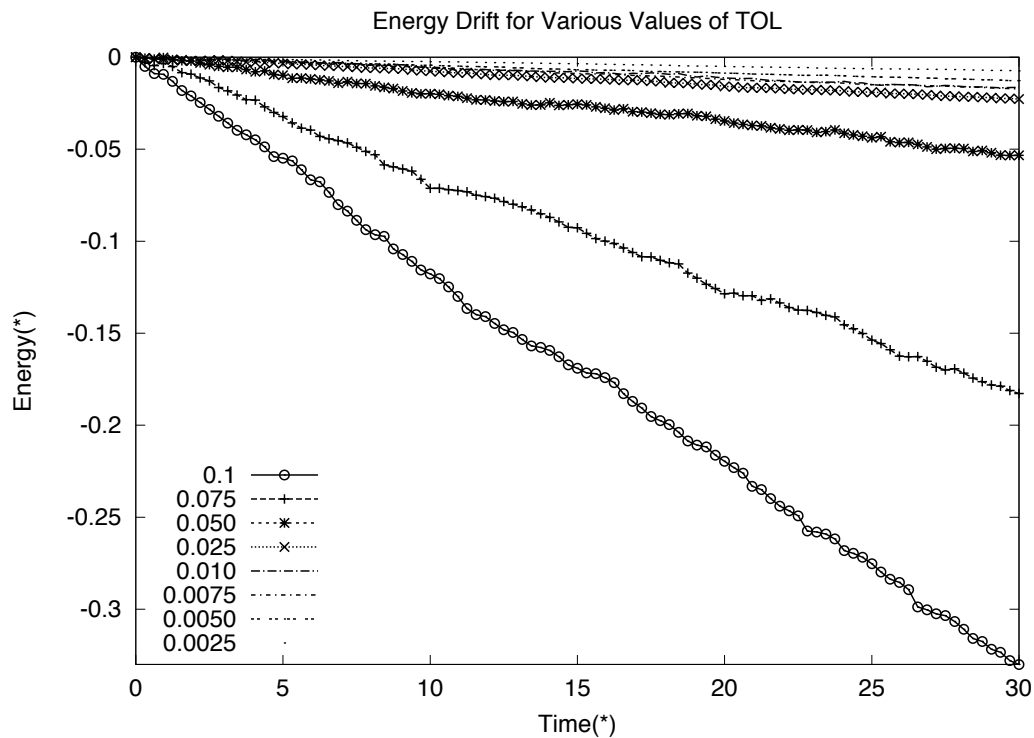


Figure 2.3: Energy drift for various values of  $TOL$ .

# Chapter 3

## An Improved Energy Drift Control

In the previous section it was shown that, when using a standard RK method, the energy drift in an MD simulation varies predictably with the parameter  $TOL$ . We present several strategies for directly controlling the energy drift over a simulation by exploiting this relationship. In addition to providing the MD practitioner with the ability to bound the absolute energy drift during integration these strategies will also bound the associated RMS error. Consider a method of stepsize selection that attempts to ensure,

$$\max_{i,j} |e(t_i) - e(t_j)| \leq \text{MAX} , \quad (3.1)$$

where  $e(t_i)$  is the energy of the simulation at time  $t_i$  and  $\text{MAX}$  is the maximum allowable energy drift, specified by the user. Under these conditions we have,

$$\begin{aligned} \epsilon_{\text{RMS}} &= \sqrt{\frac{\sum_{i=1}^M (e(t_i) - e(0))^2}{M}} \\ &\leq \sqrt{\frac{\sum_{i=1}^M \text{MAX}^2}{M}} = \text{MAX} . \end{aligned}$$

Each of our proposed algorithms operates by directly attempting to satisfy (3.1). Thus, in

subsequent sections, we are able to obtain a bound on  $\epsilon_{\text{RMS}}$  in addition to a guaranteed bound on the energy drift.

## 3.1 The Algorithms

Intuitively, each of the strategies described below bound the drift over the course of the simulation by ensuring that a given step is only accepted if the energy change over that step is not too large. We should reiterate that although RMS error is often used when comparing integrators[14], we are primarily interested in bounding the absolute energy drift since it is the physically relevant quantity. We have observed that the absolute energy drift is a more stringent condition than RMS error so, with proper care in choosing the MAX parameter, we will be able to directly compare the efficiency of our step selection strategies with the benchmark Verlet method.

### 3.1.1 Simple Energy Error Control

The first technique we propose satisfies (3.1) for  $t \in [0, t_{\text{end}}]$  by modifying the stepsize selection procedure used in the Runge-Kutta integrator (we will use rkd56 in most of the examples in this chapter). After the attempted step from  $t_{n-1}$  to  $t_n$  we accept only if

$$\frac{t_{\text{end}} \|e(t_n) - e(t_{n-1})\|}{h_n} \leq \text{MAX}, \quad (3.2)$$

where  $h_n = t_n - t_{n-1}$  is the trial stepsize. This will guarantee that the required bound is satisfied since for an arbitrary choice of  $i$  and  $j$  such that  $t_i, t_j \in [0, t_{\text{end}}]$  and  $j > i$ , we have:

$$\begin{aligned}
e(t_i) - e(t_j) &= \sum_{k=i+1}^j e(t_{k-1}) - e(t_k) \\
&\leq \sum_{k=i+1}^j \frac{\text{MAX } h_k}{t_{\text{end}}} \\
&= \text{MAX} \frac{\sum_{k=i+1}^j h_k}{t_{\text{end}}} \\
&\leq \text{MAX} .
\end{aligned}$$

In the case of rejected steps we simply adjust the trial stepsize using equation (1.6) with  $est_n$  set to the left hand side of equation (3.2). The step is then retried with the adjusted stepsize. This stepsize selection strategy does not require the use of a continuous polynomial approximation so that for each step taken by rkd56 only eight function evaluations are required per step.

### Numerical Results

In this, and subsequent numerical results sections we choose the MAX parameter to be  $1.877 \times 10^{-2}$ . This value was obtained by calculating  $\max_{i,j} |e(t_i) - e(t_j)|$ , where  $e(t_i)$  are the energies at the  $i$ th step of the benchmark Verlet simulation in chapter 2. We use 10 times the observed Verlet drift, since our algorithm ensures that the bound is strictly satisfied and since RMS error is a less restrictive measure of the quality of the simulation.

	Verlet-Stormer	Runge-Kutta
Scaled Stepsize	$4.6294 \times 10^{-4}$	$3.4960 \times 10^{-4}$
RMS Error	$5.9438 \times 10^{-4}$	$7.9098 \times 10^{-5}$
Max Energy Drift	$1.877 \times 10^{-3}$	$1.3861 \times 10^{-4}$

Table 3.1: Scaled stepsize, RMS error, and maximum energy drift for the benchmark Verlet method and the simple stepsize selection strategy applied with rkd56.

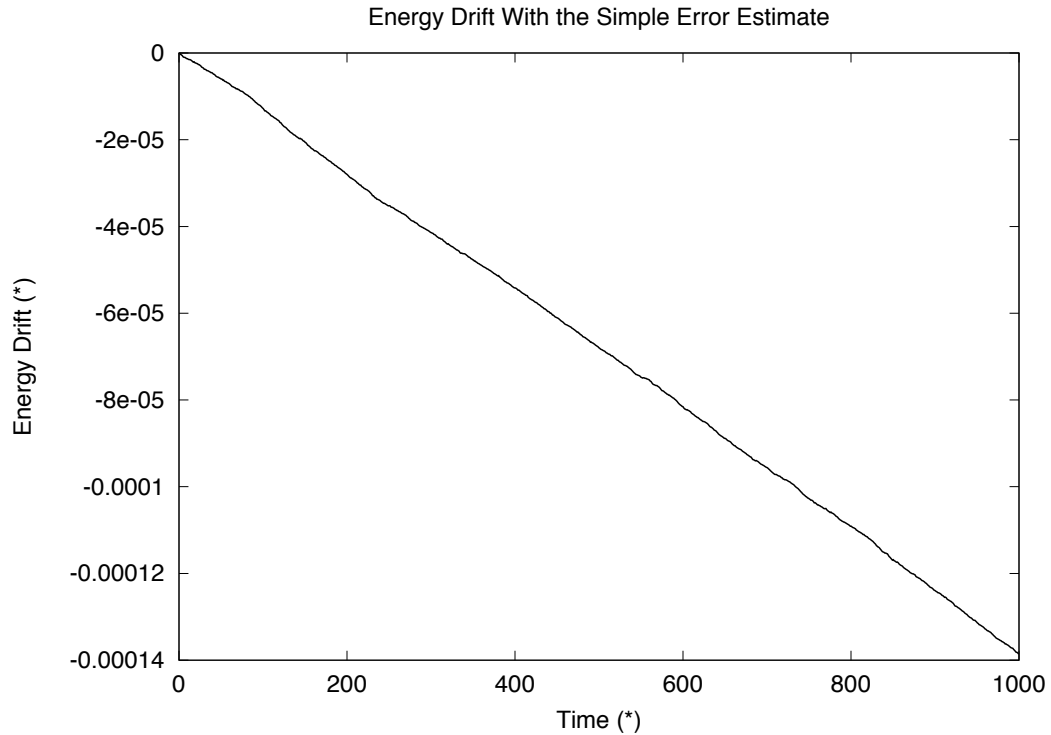


Figure 3.1: Energy drift observed with the novel stepsize selection in rdk56.

Table 3.1 summarizes the observed results for this simple stepsize selection strategy. The third row demonstrates that the bound given by (3.1) is satisfied. This strategy is somewhat overzealous in controlling the energy drift, which can be seen to be two orders of magnitude smaller than the specified value for  $MAX$ .

In terms of efficiency the proposed algorithm fares well - with a scaled stepsize thirty per cent smaller than that used in the Verlet method we see a tenfold improvement in the RMS error. Adjustments to this stepsize selection strategy in subsequent sections will further improve on these results by exploiting the fact that the observed energy drift is significantly smaller than that predicted by the  $MAX$  parameter.

### 3.1.2 Adjusting the error estimate

A consequence of the error control given by (3.2) is that after any timestep  $t_n$  we are guaranteed that  $|e(t_n) - e(0)| \leq \text{MAX} \frac{t_n}{t_{\text{end}}}$ . In practice this inequality is almost never sharp so that each step introduces wasted energy drift that could be used in subsequent steps. In this section we present our first adjustment to the simple rkd56 stepsize selection strategy that takes advantage of this wasted drift in order to increased the average step size over the integration.

On the  $n$ th step of the simulation we have  $\text{MAX} - |e(t_{n-1}) - e(0)|$  units of energy that we could use in the remainder of the run in addition to the acceptable drift as computed by the simple stepsize selection strategy (3.2). This suggests that we modify the stepsize selection strategy to accept the  $n$ th step if the energy change over that step satisfies

$$|e(t_n) - e(t_{n-1})| \leq \frac{(\text{MAX} - |e(t_{n-1}) - e(0)|)h_n}{t_{\text{end}} - t_{n-1}}. \quad (3.3)$$

If this equation is satisfied for all  $n$  then we have

$$\begin{aligned} \frac{(t_{\text{end}} - t_{n-1})|e(t_n) - e(t_{n-1})|}{h_n} &\leq \text{MAX} - |e(t_{n-1}) - e(0)| \\ |e(t_n) - e(t_{n-1})| &\leq \text{MAX} - |e(t_{n-1}) - e(0)| \end{aligned}$$

since  $\frac{t_{\text{end}} - t_{n-1}}{h_n} < 1$  so that

$$|e(t_n) - e(t_{n-1})| + |e(t_{n-1}) - e(0)| \leq \text{MAX}$$

Therefore, since the triangle inequality implies that  $|e(t_n) - e(0)| \leq |e(t_n) - e(t_{n-1})| + |e(t_{n-1}) - e(0)|$ , we have  $|e(t_n) - e(0)| \leq \text{MAX}$ . Since (3.3) guarantees that at any given point in the simulation we have  $|e(t_n) - e(0)| \leq \text{MAX}$ , the observed energy drift will remain bounded by the user-defined acceptable limit.

## Numerical Results

Applying the error control strategy (3.3) gives a characteristic energy drift as shown in figure 3.2. As the simulation progresses an increasing amount of unused drift accumulates resulting in a larger stepsize near  $t = t_{\text{end}}$ . The total energy drift is somewhat closer to the value specified by MAX, although there still remains substantial unused drift at the end of the simulation.

	Verlet-Stormer	Runge-Kutta
Scaled Stepsize	$4.6294 \times 10^{-4}$	$4.0123 \times 10^{-4}$
RMS Error	$5.9438 \times 10^{-4}$	$1.9141 \times 10^{-4}$
Max Energy Drift	$1.8770 \times 10^{-3}$	$9.2398 \times 10^{-4}$

Table 3.2: Scaled stepsize, RMS error, and maximum energy drift for the benchmark Verlet method and the adjusted stepsize selection strategy (3.3) used with rkd56.

Table 3.2 reports the improved performance of this stepsize selection strategy, as we are able to take a significantly larger average stepsize compared to the previous method. The scaled stepsize is only 15 percent smaller than that of the Verlet benchmark while the RMS error is three times smaller giving the 6<sup>th</sup> order RK method performance comparable to that of Verlet. At the end of this chapter we will demonstrate that further improvements in performance can be realized by applying this strategy to higher-order RK methods, resulting in a significant performance gain when compared to the Verlet integrator.

Although the absolute change in energy remains bounded by the parameter MAX the non-uniform behavior of the energy drift over the interval of integration may be undesirable to the MD practitioner. In the next section we propose an additional modification to the stepsize selection strategy that will increase the uniformity of the energy drift over  $[0, t_{\text{end}}]$  at the expense of introducing an additional ad-hoc parameter.

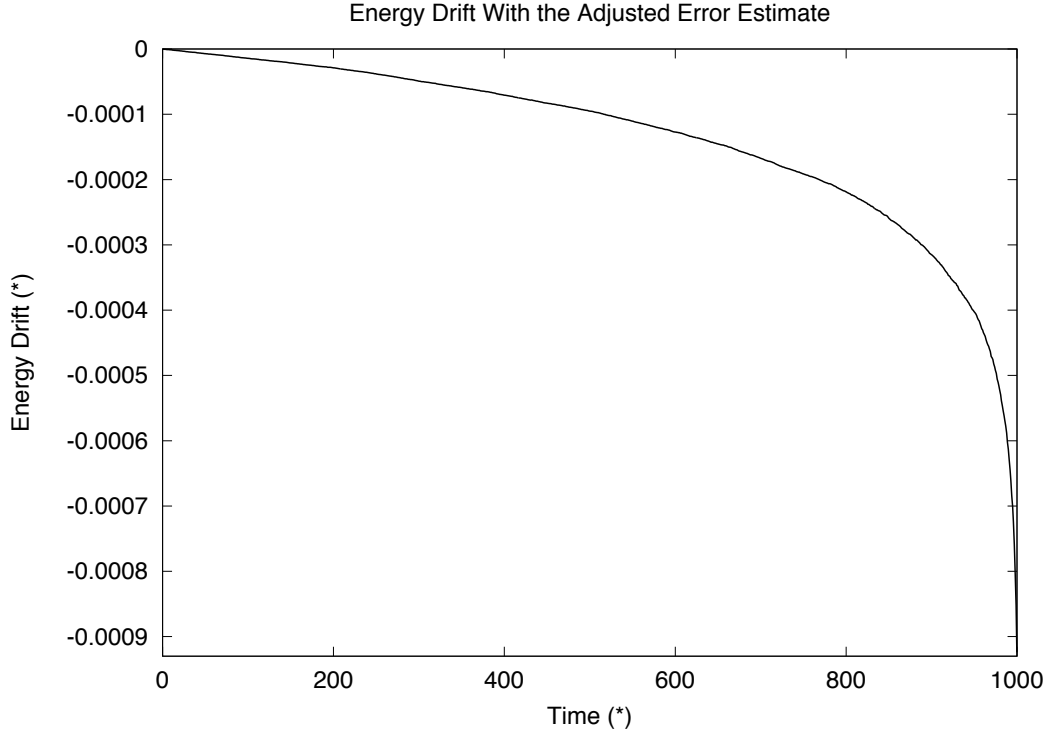


Figure 3.2: Energy drift using the stepsize selection strategy (3.3).

### 3.1.3 A further adjustment

In order to achieve greater uniformity in the energy drift as the simulation approaches  $t = t_{\text{end}}$  we propose splitting the interval  $[0, t_{\text{end}}]$  into subintervals of equal length, while applying the stepsize adjustment (3.3) over each subinterval. Formally, this involves introducing an ad-hoc parameter  $N_{\text{int}}$  to be the number of subintervals of width  $W_{\text{int}} \stackrel{\text{def}}{=} \frac{t_{\text{end}}}{N_{\text{int}}}$ . We denote the  $l^{\text{th}}$  interval by  $[t^{l-1}, t^l] \stackrel{\text{def}}{=} [(l-1)W_{\text{int}}, lW_{\text{int}}]$  for  $l \in \{1, \dots, N_{\text{int}}\}$ . For what follows, we let  $\{t_0^l, \dots, t_{M_l}^l\}$  denote the subset of all steps  $\{t_0, \dots, t_M\}$  that lie in the  $l^{\text{th}}$  subinterval. The stepsize associated with the  $t_n^l$ th step is then defined as  $h_n^l \stackrel{\text{def}}{=} t_n^l - t_{n-1}^l$ .

In order to define this alternative stepsize selection strategy we need to introduce the following additional quantity,

$$\Delta t_n^l \stackrel{\text{def}}{=} W_{\text{int}} - (t_n^l - t^{l-1}),$$

to be the time remaining in the current subinterval. For simplicity, we approximate  $e(t^{l-1})$  by using  $e(t_{M_{l-1}}^{l-1})$  for the value of the energy at the start of the interval. This does not pose a significant problem so long as  $N_{\text{int}}$  is chosen so that  $W_{\text{int}}$  is significantly larger than the average stepsize. It is possible to use the continuous approximation to the solution to calculate the energy precisely at  $t^{l-1}$ , or to truncate steps that cross a subinterval boundary but in practice each of these choices has a negligible effect on the outcome.

Finally, step  $t_n^l$  is accepted if and only if

$$\frac{|e(t_n^l) - e(t_{n-1}^l)|}{h_n^l} \leq \frac{\frac{\text{MAX}}{N_{\text{int}}} - |e(t_{n-1}^l) - e(t^{l-1})|}{\Delta t_{n-1}^l} \quad (3.4)$$

For a method satisfying equation (3.4) we have

$$\begin{aligned} \frac{|e(t_n^l) - e(t_{n-1}^l)| \Delta t_{n-1}^l}{h_n^l} &\leq \frac{\text{MAX}}{N_{\text{int}}} - |e(t_{n-1}^l) - e(t^{l-1})| \\ |e(t_n^l) - e(t_{n-1}^l)| &\leq \frac{\text{MAX}}{N_{\text{int}}} - |e(t_{n-1}^l) - e(t^{l-1})| \end{aligned}$$

since  $\frac{\Delta t_{n-1}^l}{h_n^l} < 1$ . It follows that

$$|e(t_n^l) - e(t_{n-1}^l)| + |e(t_{n-1}^l) - e(t^l)| \leq \frac{\text{MAX}}{N_{\text{int}}}$$

Therefore, since the triangle inequality implies that  $|e(t_n^l) - e(t^l)| \leq |e(t_n^l) - e(t_{n-1}^l)| + |e(t_{n-1}^l) - e(t^l)|$ , we have  $|e(t_n^l) - e(t^l)| \leq \frac{\text{MAX}}{N_{\text{int}}}$ . This inequality follows for all steps except possibly for those steps that span a subinterval boundary. By adjusting the stepsize selection strategy to ensure that the step does not enter into the next subinterval it is possible to make this equality hold for all steps. In practice, the few steps where this inequality may not be satisfied do not substantially affect the energy drift and we assume all steps are contained within the subinterval

in order to simplify the already cumbersome notation. Since the energy drift over an arbitrary subinterval is bounded by  $\frac{\text{MAX}}{N_{\text{int}}}$  we ensure that the drift over the entire integration is bounded by  $\text{MAX}$ .

In obtaining the numerical results presented in this section, we arbitrarily chose  $N_{\text{int}} = 100$  but this number could potentially be given a default value, and be updated as the simulation progresses. In any realistic MD simulation there will be billions of steps taken so choosing an appropriate  $N_{\text{int}}$  does not present a significant difficulty.

### Numerical Results

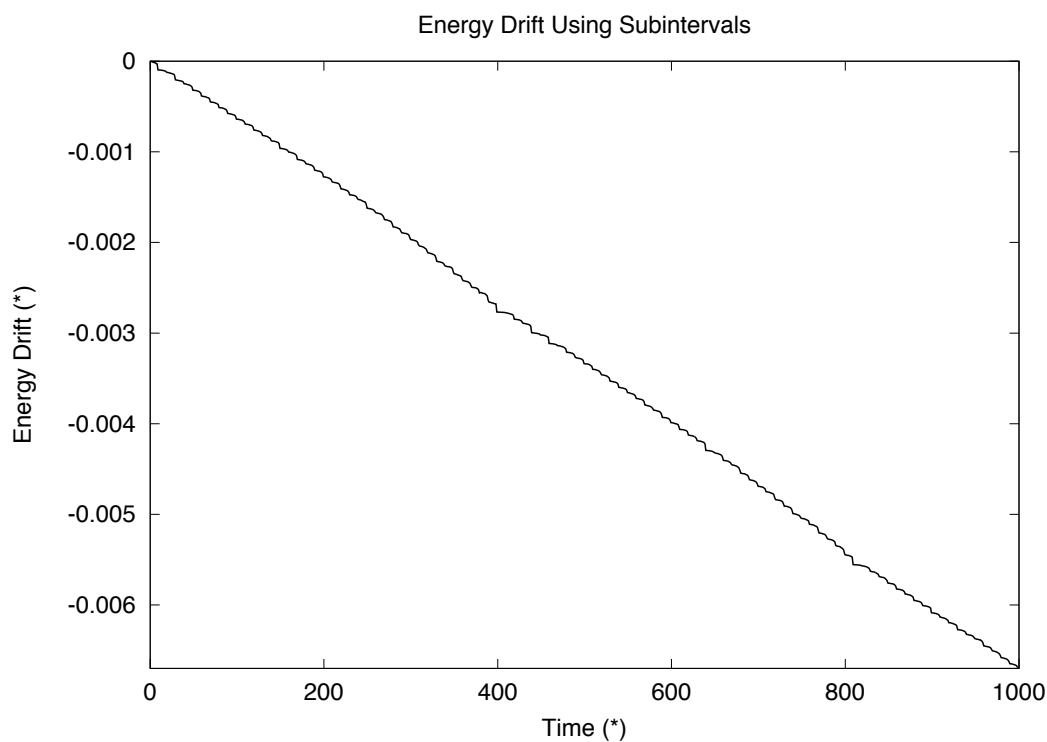


Figure 3.3: Energy drift using the stepsize selection strategy (3.4) with  $N_{\text{int}} = 100$ .

Table 3.3 reports the energy drift obtained using strategy (3.4). The modified strategy is seen to have in a six-fold increase in the energy drift which is observed to be within an order of magnitude of the predicted value. As expected, this results in increased average stepsize and

	Verlet-Stormer	Runge-Kutta
Scaled Stepsize	$4.6294 \times 10^{-4}$	$5.5112 \times 10^{-4}$
RMS Error	$5.9438 \times 10^{-4}$	$3.6323 \times 10^{-3}$
Max Energy Drift	$1.8770 \times 10^{-3}$	$6.3522 \times 10^{-3}$

Table 3.3: Scaled stepsize, RMS error, and maximum energy drift for the benchmark Verlet method and the stepsize selection strategy (3.4) applied for rkd56.

increased  $\epsilon_{\text{RMS}}$ . Since these values are substantially larger than those obtained using the Verlet method this particular simulation is difficult to compare to the benchmark in terms of efficiency and accuracy, although it is evident that our approach performs quite well in maximizing the average stepsize subject to the specified energy drift.

### 3.1.4 Higher order methods

Our previous experiments have demonstrated that novel stepsize selection strategies are able to perform comparably to the Verlet method when considering  $\epsilon_{\text{RMS}}$  and scaled stepsize for a particular order of RK formula. The closest-matched trials have shown a slightly smaller stepsize coupled with a significantly improved RMS error with respect to the benchmark simulation. In this section we determine the performance gains that can be realized by moving to an 8<sup>th</sup> order RK method with the stepsize selection strategy (3.3) described in section 3.1.2 (since this strategy proved to be most similar to Verlet in terms of performance).

### Numerical Results

There is a marked difference in the behavior of the energy drift as  $t$  tends to  $t_{\text{end}}$  when using the higher order RK method. Figure 3.4, when compared to figure 3.2, shows that the sudden increase in the observed energy drift when using lower order method is greatly reduced. The cause of this increased consistency is unclear, but we hypothesize that it is the result of the

differing values for  $p$  in (1.6). This hypothesis is supported by the fact that the  $\left(\frac{TOL}{est_n}\right)^{\frac{1}{p}}$  term is noticeably steeper for the 6<sup>th</sup> order method when  $TOL$  is close to  $est_n$ , and that the fraction of failed steps is 5% smaller for the higher order method.

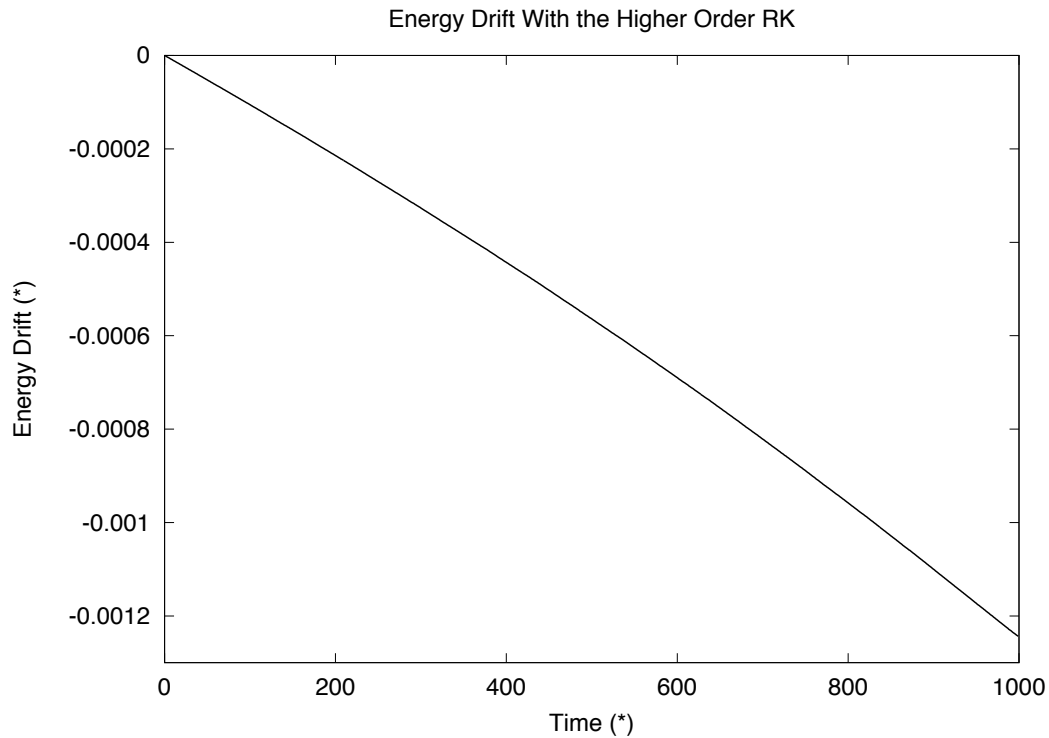


Figure 3.4: Energy drift using the 8th order RK method rkd78 and the stepsize selection strategy (3.3).

In addition to this improved qualitative behavior, table 3.4 shows that the higher order method is using a substantially larger portion of the drift provided by the parameter  $MAX$ . While we still have an order of magnitude of unused drift (recall that the value of  $MAX$  provided to the RK method is  $1.877 \times 10^{-2}$ ) the results from the 8<sup>th</sup> order method are 30 percent closer to the target value.

Perhaps the most significant improvement obtained with the higher order method is the increased efficiency. With an  $\epsilon_{RMS}$  close to the Verlet benchmark we are able to take a stepsize nearly 20 percent larger. Although RK methods are commonly cited in the literature as

	Verlet-Stormer	Runge-Kutta
Scaled Stepsize	$4.6294 \times 10^{-4}$	$5.4792 \times 10^{-4}$
RMS Error	$5.9438 \times 10^{-4}$	$6.8510 \times 10^{-4}$
Max Energy Drift	$1.8770 \times 10^{-3}$	$1.2436 \times 10^{-3}$

Table 3.4: Scaled stepsize, RMS error, and maximum energy drift for the benchmark Verlet method and the stepsize selection strategy (3.3) applied with rkd78.

being unsuitable for long MD simulations[10] [5] [17] it is evident that they can be modified to perform competitively even when compared to the commonly used symplectic methods. Since these modifications also provide the user with the novel ability to adaptively bound the total energy drift over an integration, we suggest that RK methods should not be ruled out of consideration for MD applications.

# Chapter 4

## PBC and cutoffs

### 4.1 Description

The numerical results presented in the previous chapter were computed using the full force calculation and the simplest possible boundary conditions. This results in optimal energy conservation and was useful as a best-case comparison, but it is not practical for realistic biomolecular simulations. Most biomolecular systems involve the behavior of molecules in bulk fluid, and the conditions set up in the previous chapter will create excessive simulation artifacts due to the large fraction of particles interacting with the free boundary. Further, the full force calculation is prohibitively expensive for large systems and approximations of the force must be introduced to reduce the computer time required for the force evaluations.

In practice, periodic boundary conditions (PBCs) are often used to simulate bulk matter with a small number of particles. The simulation is treated as a lattice of repeated cubical cells of width  $w_{\text{box}}$ , each cell being an exact replica of the first. As a particle leaves from one side of a cell its image from an adjacent cell enters via the opposite side, maintaining a constant number of particles per box (see Figure 4.1). Without further approximation the particles in the simulation are able to interact with particles in any other cell, resulting in an infinite number of terms in equation 1.3. As such, a method of damping the intermolecular forces to zero after

a cutoff distance  $r_{off}$  must be introduced, if one is to evaluate the forces involved in a PBC system. That is, in computing the forces on a particle at time  $t$  only the forces due to particles within  $r_{off}$  of this particle need be computed.

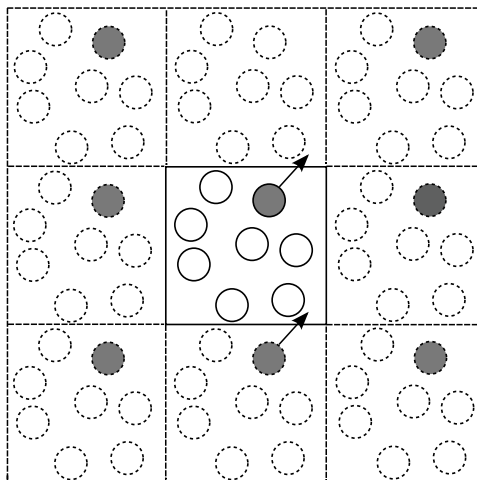


Figure 4.1: Periodic boundary conditions. As the shaded atom leaves the simulation box it's mirror image from the adjacent cell enters, maintaining a constant number of particles at all times.

The *minimum image convention* is the simplest cutoff scheme, where the  $i^{th}$  particle interacts only with nearest image of the  $j^{th}$  particle. This convention is equivalent to specifying a cutoff distance that forms a cube of width  $\frac{w_{box}}{2}$  centered at each atom. The most common switching technique used in practice is known as *spherical switching*, and involves a switching function  $s(r)$  defined to be 1 for  $r \in (-\infty, r_{on})$ , 0 for  $r \in (r_{off}, \infty)$  and decreasing monotonically from 1 to 0 for  $r \in [r_{on}, r_{off}]$  [16]. See figure 4.2 for an example of one such switching function. This function is then multiplied by the potential function  $V(r)$  or the force function  $F(r)$  to ignore the effects of particles at distances greater than  $r_{off}$ .

The *hard cutoff* method takes  $r_{on} = r_{off}$  so that the force is abruptly truncated to 0 for  $r \geq r_{off}$ . Both the minimum image convention and the hard cutoff method introduce discontinuities in the force function which create unphysical artifacts in biomolecular simulation [1]. For

this reason, and since the discontinuities introduced by these methods will cause our adaptive integrators to be less competitive, or to fail without nontrivial modification, we restrict our attention to the most commonly used switching functions with values for  $r_{on}$  and  $r_{off}$  that are generally agreed upon in the literature.

## 4.2 Potential Cutoff Scheme

We will be analyzing cutoff schemes with the switching function

$$s(r) = \begin{cases} 1 & \text{if } x < r_{on} \\ 1 + y(r)^2[2y(r) - 3] & \text{if } r_{on} \leq x \leq r_{off} \\ 0 & \text{if } x > r_{off} \end{cases}, \quad (4.1)$$

where  $y(r) = \frac{r^2 - r_{on}^2}{r_{off}^2 - r_{on}^2}$ . This switching function is used in many MD simulations [17] [16] and is one of the switching techniques included in the popular CHARMM MD package [1]. When applied as a potential switch, this function gives a continuous force function (4.2), although higher derivatives of this force function will suffer from discontinuities:

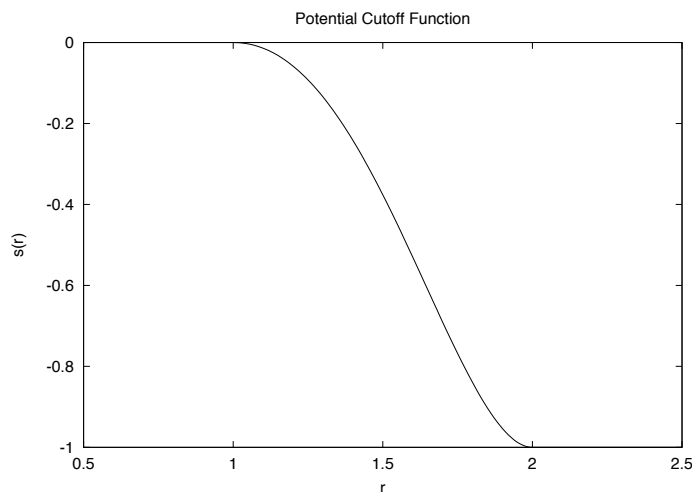


Figure 4.2: Plot of the potential cutoff function with  $r_{on} = 1$  and  $r_{off} = 2$ .

$$F(r) = \frac{d\phi(r)s(r)}{dr} = \begin{cases} \phi(r) & \text{if } x < r_{on} \\ \frac{d\phi(r)}{dr}s(r) + \frac{ds(r)}{dr}\phi(r) & \text{if } r_{on} \leq x \leq r_{off} \\ 0 & \text{if } x > r_{off} \end{cases} \quad (4.2)$$

In this equation  $\frac{ds(r)}{dr} = 6(y(r)^2 \frac{dy(r)}{dr} - y(r) \frac{dy(r)}{dr})$ ,  $\frac{dy(r)}{dr} = \frac{2r}{r_{off}^2 - r_{on}^2}$  and  $\frac{d\phi(r)}{dr}$  takes the same form as in chapter 2.

The effects of the parameters  $r_{on}$  and  $r_{off}$  in realistic biomolecular simulations have been well studied [1], [16], [17], [4]. It is generally agreed in the literature that the distance between  $r_{on}$  and  $r_{off}$  should be at least 4Å and  $r_{on}$  should be greater than or equal to 12Å. Subsequent numerical results that we determine were computed with  $r_{on} = 12\text{Å}$  and  $r_{off} = 16\text{Å}$  in order to evaluate the performance of our novel energy control strategies in a situation that is relevant to the MD community.

## 4.2.1 Standard Integrators

Initially, we apply the benchmark Verlet and standard RK methods to the PBC system outlined above. It should be noted that once cutoffs are introduced there are two possible interpretations of the energy of the system. The first is to consider the energy calculated using the modified potential function, with cutoffs. The second possibility is to consider the modified system an inexact approximation to the true system, and use the original function without cutoffs when calculating the energy.

The modified energy, modified potential and modified forces are subsequently referred to as  $E$ ,  $V$  and  $F$ , while the unmodified counterparts are denoted by  $E_{true}$ ,  $V_{true}$  and  $F_{true}$ . We subsequently examine the implications of each interpretation and how they relate to the quality of the appropriate solution.

## Numerical Results

Figure 4.3 demonstrates the typical behavior of the modified and true energy drift using the Verlet and sixth order standard RK integrators. It can be seen that, when using the modified energy, the qualitative behavior of the two methods is consistent with the observations from previous chapters. The Verlet method exhibits its characteristic oscillatory behavior and the RK method demonstrates a smooth, steady drift over the course of integration.

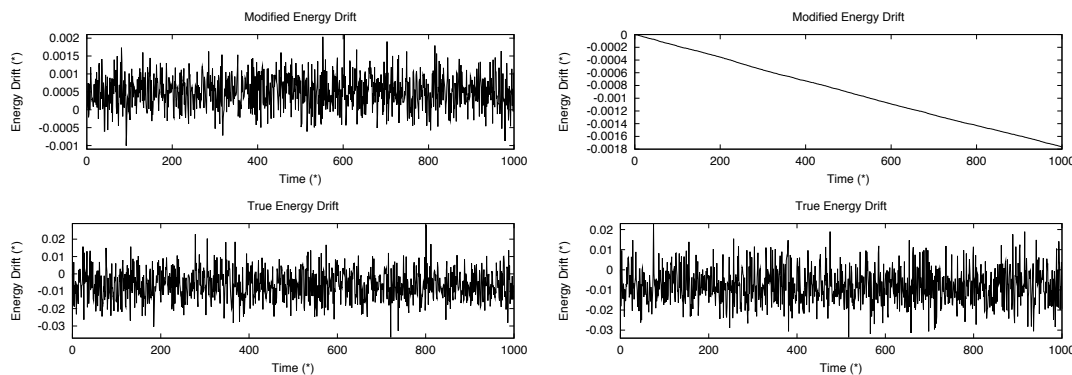


Figure 4.3: Modified energy drift (top) and true energy drift (bottom) using the Verlet integrator (left) and the rkd56 integrator (right) using the potential cutoff scheme with  $r_{on} = 12\text{\AA}$  and  $r_{off} = 16\text{\AA}$

However, when the true energy is used as a measure of the qualitative behavior of the energy drift, the situation changes substantially. Although the Verlet integrator still displays its typical oscillatory behavior, the amplitude of the oscillations are an order of magnitude larger. This increased error in the energy drift is also seen in the RK integration, so that the comparatively small extra energy drift due to the RK integration is almost negligible.

Table 4.1 shows the  $\epsilon_{\text{RMS}}$  and maximum energy drifts for the two methods using both interpretations of the energy. The columns corresponding to the true energy drift are seen to have  $\epsilon_{\text{RMS}}$  and drift values that are nearly the same for the two integrators, while this is not the case when considering the modified energy columns. We will report only the performance measures related to the modified energy in subsequent sections. Note that when using an energy

	Verlet, True	Verlet, Modified	RKD56, True	RKD56, Modified
Scaled Stepsize	$4.6294 \times 10^{-4}$	$4.6294 \times 10^{-4}$	$5.4722 \times 10^{-4}$	$5.4722 \times 10^{-4}$
RMS Error	$1.0852 \times 10^{-2}$	$6.9155 \times 10^{-4}$	$1.1944 \times 10^{-2}$	$1.0344 \times 10^{-3}$
Max Energy Drift	$6.4864 \times 10^{-2}$	$3.0934 \times 10^{-3}$	$5.6491 \times 10^{-2}$	$1.7675 \times 10^{-3}$

Table 4.1: Results for the Verlet and rkd56 methods with a potential cutoff function. Both the true, and modified energy are presented for comparison.

preserving method with a modified approximate force function one can only expect to observe the preservation of  $E$  rather than  $E_{true}$ .

## 4.2.2 Novel Integrators

In analyzing the performance of energy-based stepsize selection using PBCs, the stepsize selection strategy outlined in section 3.1.2 was used. Although this strategy was not as efficient as the one presented in section 3.1.3 it has the advantage of producing a scaled stepsize comparable to the one used in the benchmark Verlet integrations. Since it is not possible to directly estimate the scaled stepsize before a simulation is complete, this choice will allow us to most accurately determine the relative performance of the novel stepsize selection scheme. All parameters for the integration were left to the values from chapter 3, unless otherwise stated.

### Numerical Results

Table 4.2 shows the results of the novel stepsize selection strategy when used with the 6<sup>th</sup> and 8<sup>th</sup> order RK methods. Plots of the energy drift are not included here since the qualitative behavior is identical to that seen in the top right pane of figure 4.3. With a potential cutoff function the 6<sup>th</sup> order RK method significantly outperforms the 8<sup>th</sup> order integrator. This observation is consistent with the fact that the potential cutoff introduces discontinuities in the higher order derivatives of the force function.

The introduction of a potential cutoff function substantially reduces the effectiveness of the higher order RK integrators. While the 6<sup>th</sup> order method is able to perform comparably to the Verlet benchmark, the 8<sup>th</sup> order method is forced to take a scaled stepsize that is only half the size<sup>1</sup>. In each case the energy conservation is noticeably worse than that seen in previous sections. In the next section it will be shown that this degradation in performance relative to what was seen in chapter 3 is due to the introduction of discontinuities in the lower-order derivatives of the associated force function, and this can be corrected.

	RKD56	RKD78
Scaled Stepsize	$4.0708 \times 10^{-4}$	$2.5746 \times 10^{-4}$
RMS Error	$1.5893 \times 10^{-3}$	$1.3812 \times 10^{-3}$
Max Energy Drift	$7.8743 \times 10^{-3}$	$7.9312 \times 10^{-3}$

Table 4.2: Performance of novel integration schemes using a potential cutoff

### 4.3 Force cutoff

The cutoff function (4.1) can also be applied to the force function directly. Although potential cutoff schemes are more commonly used in practice, force function cutoffs have the advantage that they can be used to separate the distinct time-scales inherent in biomolecular systems [15], resulting in increased computational efficiency. Since the presence of an additional continuous derivative of the force function will likely have an effect on the performance of high-order integrators we analyze the performance of our proposed stepsize selection strategies when applied to a system with force cutoffs.

When a force cutoff is used, the potential energy of the modified system must be calculated by integrating the modified force function:

---

<sup>1</sup>This is the result of the reduced observed order of high order RK methods when solving a problem with discontinuous low order derivatives, while still using the larger number of stages associated with a high order RK method.

$$V(r) = \begin{cases} V_{true}(r) + \Delta V & \text{if } x \leq r_{on} \\ - \int_{r_{off}}^r s(r') F_{true}(r') dr' & \text{if } r_{on} < x \leq r_{off} \\ 0 & \text{if } x > r_{off} \end{cases} \quad (4.3)$$

Here,  $\Delta V$  is chosen to obtain continuity of  $V(r)$ . In our case  $\Delta V \approx 8.5904 \times 10^{-4}$  and the integral in (4.3) was computed using symbolic integration in Mathematica to be

$$-\frac{32.839}{r^{-12}} + \frac{8.7614}{r^{-10}} - \frac{0.68888}{r^{-8}} + \frac{32.857}{r^{-6}} - \frac{10.951}{r^{-4}} + \frac{1.3777}{r^{-2}} + 5.3246 \times 10^{-2} \log r$$

Again, the parameters for the numerical experiments in this section are identical to those used in chapter 3.

### 4.3.1 Standard Integrators

The benchmark Verlet and standard RK methods are again applied to the PBC system, with the force function cutoff described above. The same qualitative behavior between the two methods and two interpretations for energy as seen in figure 4.3 were observed, and the plot of the energy drift is not duplicated here. The energy error introduced by the force function approximation is again seen to dominate the effects of the integrators so that it is appropriate to determine comparative performance by exclusively using the modified energy measures.

### Numerical Results

Table 4.3 shows substantial similarity with the results obtained using the potential cutoff function. The true energy drifts are an order of magnitude greater than the modified energy drifts, and the relative performance of the two integrators cannot be determined using the true energy. Using the modified energy, the RK method again performs comparably to the Verlet benchmark with a slightly smaller stepsize taken to achieve a slightly greater  $\epsilon_{RMS}$  and smaller maximum energy drift.

	Verlet, Modified	Verlet, True	RKD56, Modified	RKD56, True
Scaled Stepsize	$4.6294 \times 10^{-4}$	$4.6294 \times 10^{-4}$	$4.5254 \times 10^{-4}$	$4.5254 \times 10^{-4}$
RMS Error	$5.4317 \times 10^{-4}$	$1.3915 \times 10^{-2}$	$1.0198 \times 10^{-3}$	$1.2749 \times 10^{-2}$
Max Energy Drift	$3.1618 \times 10^{-3}$	$8.0515 \times 10^{-2}$	$1.7637 \times 10^{-3}$	$8.8655 \times 10^{-2}$

Table 4.3: Results for the Verlet and rkd56 methods with a force cutoff function. Both the true and modified energy are presented for comparison.

### 4.3.2 Novel Integrators

The stepsize selection strategy described in section 3.1.2 was again used in order to obtain valid comparisons with the previous chapter. Both 6<sup>th</sup> and 8<sup>th</sup> order RK methods are subsequently compared. Unless otherwise stated all integration parameters were left to the values specified in chapter 3.

#### Numerical Results

Table 4.4 contains the results of the novel stepsize strategy when using the force cutoff function. The 6<sup>th</sup> order integrator took a slightly smaller timestep than in the previous section, but obtained an  $\epsilon_{\text{RMS}}$  smaller than the Verlet benchmark by a factor of two. Likewise, the maximum energy drift over the interval was nearly an order of magnitude smaller. Due to the difference in the scaled stepsize it is difficult to draw definitive conclusions about the performance under the force cutoff.

	RKD56	RKD78
Scaled Stepsize	$3.4032 \times 10^{-4}$	$4.6370 \times 10^{-4}$
RMS Error	$2.4697 \times 10^{-4}$	$7.7165 \times 10^{-4}$
Max Energy Drift	$1.3245 \times 10^{-3}$	$1.3607 \times 10^{-3}$

Table 4.4: Performance of novel integration schemes using a force cutoff

The data associated with the 8<sup>th</sup> order RK method provides more conclusive evidence that an increase in the number of continuous derivatives of the force function can improve the performance. With a stepsize slightly larger than the benchmark Verlet method it was possible to obtain an  $\epsilon_{\text{RMS}}$  nearly identical to that seen using Verlet, and a maximal energy drift less than half the size.

## 4.4 $C^\infty$ cutoffs

The previous results suggest that increasing the number of continuous derivatives in the cutoff function will improve the performance of the higher order integrators. It is possible to test this hypothesis using a slight modification to the “bump” function commonly used in functional analysis. Using the classical  $C^\infty$  function

$$f(r) = \begin{cases} e^{-\frac{1}{r^2}} & \text{if } r > 0 \\ 0 & \text{if } r \leq 0 \end{cases}$$

an associated  $C^\infty$  cutoff function can be defined with (4.2) and  $s(r)$  given by:

$$s(r) = \begin{cases} \frac{f(r_{\text{off}}-|r|)}{f(|r|-r_{\text{on}})+f(r_{\text{off}}-|r|)} & \text{if } r > r_{\text{on}} \\ 1 & \text{if } r \leq r_{\text{on}} \end{cases} \quad (4.4)$$

It is easy to show that this cutoff function  $\in C^\infty$ , and evaluates to 0 for  $r > r_{\text{off}}$  and 1 for  $r < r_{\text{on}}$  [13]. When this smooth cutoff is applied to the potential function the force can be calculated, as it was for (4.2), with

$$\frac{ds(r)}{dr} = \begin{cases} \frac{-\frac{df}{dr}(r_{\text{off}}-r)[f(|r|-r_{\text{on}})+f(r_{\text{off}}-|r|)] - [\frac{df}{dr}(|r|-r_{\text{on}}) - \frac{df}{dr}(r_{\text{off}}-|r|)]f(r_{\text{off}}-|r|)}{[f(|r|-r_{\text{on}})+f(r_{\text{off}}-|r|)]^2} & \text{if } r > r_{\text{on}} \\ 0 & \text{if } r \leq r_{\text{on}} \end{cases},$$

and

$$\frac{df(r)}{dr} = \begin{cases} \frac{2}{r^3} e^{-\frac{1}{r^2}} & \text{if } r > 0 \\ 0 & \text{if } r \leq 0 \end{cases}.$$

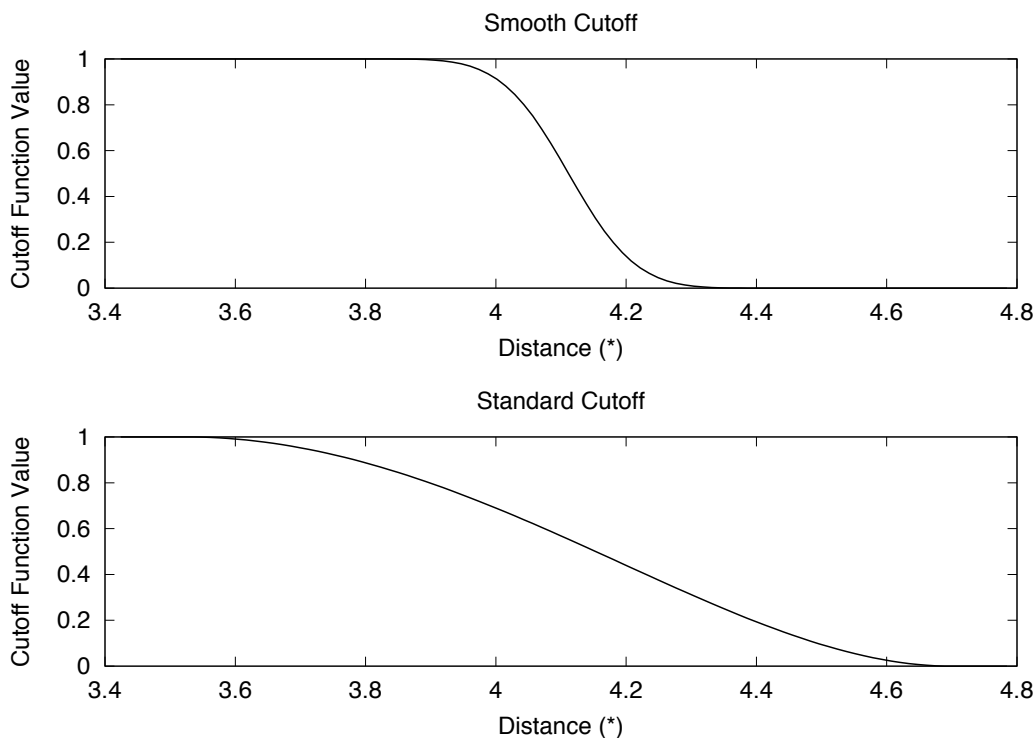


Figure 4.4: The smooth  $C^\infty$  cutoff function (top) and the standard potential cutoff function (bottom).

To our knowledge, the performance of this cutoff function in a biomolecular context has not been evaluated in the MD literature. With the values  $r_{on} = 3.5242^*$  and  $r_{off} = 4.6990^*$  (discussed in section 4.2) the  $C^\infty$  cutoff is sharper than the standard cutoff function considered earlier, and may introduce physically unrealistic forces near the cutoff boundary. However, this function is sufficient for our purposes and can be used to demonstrate the effectiveness of our stepsize selection strategies. There are other related modifications to (4.4) that could potentially improve the physical realism of the truncated force evaluations. Further, the appropriateness of these modifications can be verified using the methods presented in [16] although that is beyond

the scope of this thesis.

### Numerical Results

In order to closely match the energy drift seen in the Verlet integration, the  $\text{MAX}$  parameter was given a value of  $6.4309 \times 10^{-3}$  when using both sixth and eight order modified RK methods. This value was determined by performing two integrations with the higher order method, one with  $\text{MAX} = 1.877 \times 10^{-3}$  and the other with  $\text{MAX} = 1.877 \times 10^{-2}$ . A corresponding tenfold increase in the energy drift was observed. The final value for  $\text{MAX}$  was chosen to match the energy drift for the Verlet run by assuming that the observed energy drift depends linearly on  $\text{MAX}$ .

	Verlet	RKD56	RKD78
Scaled Stepsize	$4.6370 \times 10^{-4}$	$3.7303 \times 10^{-4}$	$5.0652 \times 10^{-4}$
RMS Error	$7.2571 \times 10^{-4}$	$4.0646 \times 10^{-4}$	$1.5694 \times 10^{-3}$
Max Energy Drift	$2.6543 \times 10^{-3}$	$1.0814 \times 10^{-3}$	$2.7522 \times 10^{-3}$

Table 4.5: Performance of novel integration schemes using a  $C^\infty$  potential cutoff

Table 4.5 demonstrates an improvement in the performance of our stepsize selection strategies when applied with an increased number of continuous derivatives in the cutoff function. The value for  $\text{MAX}$  above can be seen to provide an energy drift very close to that observed in the Verlet integration. For a maximum energy drift on the order of that seen when using the Verlet method it is possible to take a 10% larger scaled timestep with the higher order method.

Again, the 6<sup>th</sup> order RK method is outperformed by its higher order counterpart. It is interesting to note that with the  $C^\infty$  cutoff function the 6<sup>th</sup> order performs only slightly better than it did with the force cutoff, whereas the 8<sup>th</sup> order method demonstrates improvement. This is consistent with the hypothesis that the decreased performance seen with previous cutoffs was due to order reduction, and demonstrates that some care must be taken in choosing appropriate cutoff functions when applying high order integrators to molecular dynamics simulations.

# Chapter 5

## Conclusions and Future Work

### 5.1 Summary

In this paper we have developed several stepsize selection strategies that can be used with a variable stepsize Runge Kutta integrators to directly control the energy drift in a molecular dynamics simulation. These methods provide the MD practitioner with the ability to bound the total energy drift over the course of a simulation, and are able to do so in a computationally efficient manner. When applied to a modified system with a  $C^\infty$  force function, the higher order RK methods can outperform the widely used Verlet method. Discontinuities in the derivatives of the approximate force function were found to significantly effect the performance of the higher order methods, although they were able to perform comparably to the Verlet benchmark when force cutoffs were used.

The simplest stepsize selection strategy presented herein was found to significantly overestimate the energy drift in a simulation, which resulted in an unnecessarily small scaled stepsize. We presented two modifications to this strategy that were able to improve on the achievable energy drift. The first method is able to increase the scaled stepsize substantially by keeping track of the unused drift as the simulation progresses. This results in improved performance by increasing the stepsize towards the end of the integration.

It was possible to achieve a more consistent energy drift by introducing an additional ad-hoc parameter splitting the integration into distinct subintervals. The energy drift over each interval, and over the entire integration was monitored in each interval resulting in another substantial performance boost. Finally, this approach resulted in a far more uniform energy drift over the interval as a whole.

## 5.2 Future Work

There are several promising areas for future research that extend the results presented herein. One area to investigate involves mirroring the work previously done in developing variable stepsize symplectic integration methods [15]. Since these methods involve splitting the MD system into distinct timescales using a force cutoff function, it should be possible to capitalize on the good performance observed with our method when using a force cutoff. It is not entirely clear how the energy drift would be distributed between the different timescales, and some experimentation would be needed to find a reasonable resolution of this difficulty.

With GPU computing gaining more widespread use in molecular dynamics simulation the achievable timescale has increased tenfold [3]. Since the systematic energy drift experienced by non symplectic methods will be more problematic for longer time intervals it will be necessary to determine whether or not the performance of our novel strategies is able to stay feasible. In many of the experiments presented in this thesis there was significant leeway for our method to remain competitive so it is quite possible that the methods presented herein will be applicable to simulations run on GPU clusters.

Finally, it may be possible to exploit the continuous approximation to the solution given by rkd56 and rkd78 in order to salvage some of the work done on failed timesteps. In our experiments it was noted that the vast majority of failed steps did not greatly exceed the required energy bound. For the cost of a small number of additional function evaluations it may be possible to use a large fraction of the work done over failed steps which could lead to a further

improvement in performance.

# Bibliography

- [1] Brooks BR Et al. CHARMM: The biomolecular simulation program. *Journal of Computational Chemistry*, 30:1545–1615, 2009.
- [2] Shaw DE Et. al. Anton, a special-purpose machine for molecular dynamics simulations. *Communications of the ACM*, 51:89–97, 2008.
- [3] Stone E Et al. Accelerating molecular modeling applications with graphics processors. *Journal of Computational Chemistry*, 28:2618 – 2640, 2007.
- [4] Guillot B. A reappraisal of what we have learnt during three decades of computer simulations on water. *Journal of Molecular Liquids*, 101:219 – 260, 2002.
- [5] Leimkuhler B and Reich S. *Simulating Hamiltonian Dynamics*. Cambridge University Press, United Kingdom, 2004.
- [6] Cottrell D and Tupper PG. Energy drift in molecular dynamics simulations. *BIT Numerical Mathematics*, 47(3):507 – 523, 2007.
- [7] Enright WH, Jackson KR, Nørsett SP and Thompsen PG. Interpolants for Runge-Kutta formulas. *ACM Transactions on Mathematical Software*, 12(3):193 – 218, 1986.
- [8] Benettin G and Giorgilli A. On the Hamiltonian interpolation of near-to-the-identity symplectic mappings with application to symplectic integration algorithms. *Journal of Statistical Physics*, 74:1117–1143, 1994.

- [9] Berendsen HJ and van Gunsteren WF. *In Molecular Dynamics Simulations of Statistical Mechanical Systems, Proceedings of the Enrico Fermi Summer School, pp. 43.* Soc. Italiana de Fisica, Bologna Italy, 1985.
- [10] Haile JM. *Molecular Dynamics Simulation: Elementary Methods.* John Wiley and Sons, New York, 1992.
- [11] Verlet L. Computer experiments on classical fluids. *Physics Review*, 159:98 – 103, 1967.
- [12] Yan L. Robust and reliable defect control for runge-kutta methods. Master's thesis, Department of Computer Science, University of Toronto, 2005.
- [13] Fry R and McManus S. Smooth bump functions and the geometry of banach spaces. a brief survey. *Expositiones Mathematicae*, 20:143–183, 2002.
- [14] Skeel RD and Okunbor D. Canonical numerical methods for molecular dynamics simulations. *Journal of Computational Chemistry*, 15:72 – 79, 1994.
- [15] Skeel RD and Biesiadecki JJ. Symplectic integration with variable stepsize. *Annals of Numerical Mathematics*, 1:1–9, 1994.
- [16] PJ Steinback and Brooks BR. New spherical-cutoff methods for long-range forces in macromolecular simulation. *Journal of Computational Chemistry*, 15:667–683, 1994.
- [17] Schlick T. *Molecular modeling and simulation : an interdisciplinary guide.* Springer., New York, 2002.
- [18] Enright WH. A new error-control for initial value solvers. *Applied Mathematics and Computation*, 31:288 – 301, 1989.
- [19] Enright WH. The relative efficiency of alternative defect control schemes for high-order continuous Runge-Kutta formulas. *SIAM Journal on Numerical Analysis*, 30(5):1419 – 1445, 1993.

- [20] Jorgensen WL and Tirado-Rives J. Potential energy functions for atomic-level simulations of water and organic and biomolecular systems. *Proc. Nat. Acad. Sci.*, 102:6665 – 6670, 2005.